AFRL-SN-RS-TR-2005-411
Final Technical Report
January 2006

INTELLIGENT SIGNAL PROCESSING FOR INTEGRATED SENSOR SYSTEM

University of New Orleans

APPROVED FOR PUBLIC RELEASE; DISTRIBUTION UNLIMITED.

AIR FORCE RESEARCH LABORATORY
SENSORS DIRECTORATE
ROME RESEARCH SITE
ROME, NEW YORK

STINFO FINAL REPORT

This report has been reviewed by the Air Force Research Laboratory, Information Directorate, Public Affairs Office (IFOIPA) and is releasable to the National Technical Information Service (NTIS). At NTIS it will be releasable to the general public, including foreign nations.

AFRL-SN-RS-TR-2005-411 has been reviewed and is approved for publication

APPROVED: /s/

BRAHAM HIMED
Project Engineer

FOR THE DIRECTOR: /s/

RICHARD G. SHAUGHNESSY, Chief
Rome Operations Office
Sensors Directorate

REPORT DOCUMENTATION PAGE

Form Approved
OMB No. 074-0188

1. AGENCY USE ONLY (Leave blank)	2. REPORT DATE	3. REPORT TYPE AND DATES COVERED
	JANUARY 2006	Final SEP 03 – AUG 04

4. TITLE AND SUBTITLE
INTELLIGENT SIGNAL PROCESSING FOR INTEGRATED SENSOR SYSTEM

5. FUNDING NUMBERS
C - F30602-03-2-0263
PE - 62204F
PR - 517R
TA - 15
WU - 04

6. AUTHOR(S)
Braham Himed and
Hai Deng

7. PERFORMING ORGANIZATION NAME(S) AND ADDRESS(ES)
University of New Orleans
Department of Electrical Engineering
New Orleans Louisiana 70148

8. PERFORMING ORGANIZATION REPORT NUMBER
N/A

9. SPONSORING / MONITORING AGENCY NAME(S) AND ADDRESS(ES)
Air Force Research Laboratory/SNRT
26 Electronic Parkway
Rome New York 13441-4514

10. SPONSORING / MONITORING AGENCY REPORT NUMBER
AFRL-SN-RS-TR-2005-411

11. SUPPLEMENTARY NOTES

AFRL Project Engineer: Braham Himed/SNRT/(315) 330-2551/ Braham.Himed@rl.af.mil

12a. DISTRIBUTION / AVAILABILITY STATEMENT
APPROVED FOR PUBLIC RELEASE; DISTRIBUTION UNLIMITED.

12b. DISTRIBUTION CODE

13. ABSTRACT ***(Maximum 200 Words)***

New robust and efficient techniques to effectively detect ground moving targets in the presence of severe clutter and jamming environments are introduced. The first is an Image Feature Based Space Time Processing (IFSTP) algorithm. This new approach exploits the distinct image features of targets and interference signals in the angle-Doppler domain. An image segmentation algorithm, referred to as Region Growing (RG), extracts targets and interference features in the angle-Doppler domain, and an innovative block-size detection algorithm discriminates between moving targets and interference based on the extracted image features. The second uses a novel waveform scheme to concurrently extract target range and Doppler information. A pair of orthogonal waveforms with different pulse repetition frequencies (PRF) are bundled and transmitted as a single hybrid radar waveform for target measurement. At the receiver, two orthogonal signal processing channels consisting of a low PRF and high PRF channel, perform the extraction of target range and Doppler information, respectively. The CLEAN algorithm is innovatively used to suppress the interference form the cross-correlation residues and the auto-correlation sidelobe in the LPRF channel.

14. SUBJECT TERMS
Space-Time Processing, Image Processing, Region Growing, Orthogonal Waveforms, Waveform Diversity, Radar Range, Radar Doppler, CLEAN Algorithm

15. NUMBER OF PAGES
48

16. PRICE CODE

17. SECURITY CLASSIFICATION OF REPORT	18. SECURITY CLASSIFICATION OF THIS PAGE	19. SECURITY CLASSIFICATION OF ABSTRACT	20. LIMITATION OF ABSTRACT
UNCLASSIFIED	UNCLASSIFIED	UNCLASSIFIED	UL

Table of Content

List of Figures

List of Tables

Abstract

An Image Feature Based Space Time Processing (IFSTP) algorithm is introduced to effectively detect moving ground targets in clutter and jamming via airborne radar. This new approach exploits the distinct image features of targets and interference signals in the angle-Doppler domain. An image segmentation algorithm, referred to as Region Growing (RG), extracts targets and interference features in the angle-Doppler domain, and an innovative block-size detection algorithm discriminates between moving targets and interference based on the extracted image features. The proposed IFSTP algorithm is particularly suitable for detecting ground moving targets in highly non-homogeneous clutter environments, without any requirement for clutter covariance estimation.

PART I: IMAGE FEATURE-BASED SPACE TIME PROCESSING FOR GROUND MOVING TARGET DETECTION

1. Introduction

Space Time Adaptive Processing (STAP) has been widely used in advanced airborne and space-based radar systems to detect ground moving targets embedded in heavy clutter and jamming environments [1-5]. Joint space-time processing is necessary for ground clutter rejection because the ground clutter couples between the spatial domain and the time domain due to platform motion. However, successful implementation of STAP requires accurate real-time estimation of the clutter covariance matrix. The "training" data used for clutter estimation is normally obtained by sampling secondary cells that are spatially adjacent to the primary detection cell, with the assumption that the clutter in the primary and secondary cells is statistically Independent and Identically Distributed (IID) [1-3]. Moreover, the accuracy of the clutter estimate depends upon the number of available IID secondary data [1]. Since ground clutter is non-homogeneous, finding sufficient IID secondary data for detection processing poses the most serious challenge to successfully implementing STAP algorithms. Even though rank-reduction approaches such as partially adaptive STAP or subspace-based STAP can lessen the requirements on secondary data [3, 4], target detection using STAP is still contingent upon the availability of sufficient IID secondary data. In some extreme situations, no IID secondary data may be available, which severely limits the effectiveness of traditional STAP methods. This paper develops a novel space-time processing algorithm, termed Image Feature Based Space-Time Processing (IFSTP), for

effective ground moving target detection in non-homogeneous clutter environment without using any secondary data.

2. Image Feature-Based Space-Time Processing (IFSTP)

Consider an airborne sensor system that collects echo data in the space-time domain by transmitting multiple coherent pulses and receiving data from each element of an antenna array. STAP suppresses interference by "whitening" interference signals and further integrates target signals through two-dimensional matched filtering in the time-space domain [5]. The proposed IFSTP technique, however, transforms the collected space-time data directly into the angle-Doppler domain; hence, both target signal and interference are coherently integrated through the transform. The discrimination processing of targets and interference signals for detection processing is performed based on their different features in the angle-Doppler plane without explicitly filtering out interference signals.

Figure 1 shows a typical target-and-interference image of a detection cell in the angle-Doppler plane for an airborne radar system.

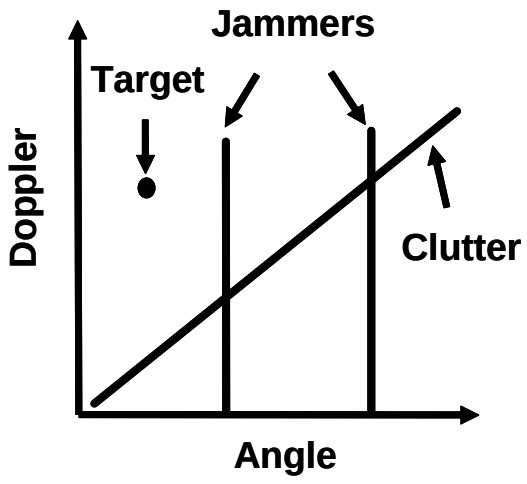

Figure 1: Typical target and interference scene image on the angle-Doppler plane for airborne radar systems

If the number of transmitted pulses during a Coherent Processing Interval (CPI) and the number of array elements are large enough, the target signal becomes a concentrated point in the transform domain. Jamming is strongly correlated in the angle domain, but completely random in the Doppler domain. Consequently, as shown in Fig. 1, jammer signals in the angle-Doppler plane are straight lines parallel to the Doppler axis. Due to the coupling between the space and time domains through antenna sidelobes, ground clutter is linearly extended in both angle and Doppler domains. As a result, clutter normally manifests itself as a tilted ridge or even multiple parallel ridges depending on the ratio of the platform speed to the radar Pulse Repetition Frequency (PRF). Thermal noise, not shown in Fig. 1, is uncorrelated in both the space and time domains, and thus statistically uniformly spread in the angle-Doppler plane through the 2-D Fourier transform. Therefore, in the angle-Doppler domain, the structure of target signals is conspicuously different from that of ground clutter or jamming, i.e. target signals are concentrated while interference is extended. Note that moving target signals generally do not overlap with clutter on the angle-Doppler plane because of their different Doppler frequencies. Hence, based on the above observations, we develop the IFSTP algorithm for automatic discrimination of moving target signals from interference in the angle-Doppler domain.

The first step of IFSTP is to transform radar data collected in the space-time domain to an image in the angle-Doppler domain through a two-dimensional Fourier transformation. Subsequently, a clamping processing is applied to all pixels of the transformed images to remove white noise. The value of a pixel is set to zero if its magnitude is smaller than a pre-defined threshold; otherwise, the pixel remains

unchanged and is labeled as a non-zero pixel. The threshold level *T* used in the clamping processing is derived from the standard deviation of the transformed white noise,

$$T = C \cdot \sigma_n \tag{1}$$

where *C* is a constant that normally is chosen to be between 2 and 3, and σ_n is the standard deviation of the white noise, which is mainly generated in the radar receiver [6].

Following the clamping processing, the remaining non-zero pixels are either target signals or interference (clutter or jamming). Feature extraction from the clamped image is carried out by clustering non-zero pixels into pixel blocks consisting of consecutively connected non-zero pixels through an image segmentation algorithm called *region growing* [7, 8]. The growing of a pixel block is implemented by comparing the ranges between the pixel block and nearby pixels with a pre-defined growing distance *D*. The range *R* between a pixel *q* and a pixel block consisting of *L* pixels $\{p_0, p_1, \Lambda\ p_L\}$ is defined as the minimum distance between pixel *q* and any pixel in the block:

$$R = \min_i \| p_i, q \|,\ 1 \le i \le L \tag{2}$$

The region growing procedure we developed for IFSTP is detailed as follows:

Step 1: Choose any non-zero pixel p_0^i as an initial element of block B_i, i.e.

$$B_i = \{p_0^i\}, i = 0$$

Step 2: Grow B_i by merging all non-zero pixels $p_1^i, p_2^i, \Lambda\ , p_L^i$ whose ranges to B_i are not larger than the pre-defined growing distance *D*, i.e.

$$B_i \Leftarrow B_i \cup \{p_1^i, p_2^i, \Lambda\ , p_L^i\} \tag{3}$$

Step 3: Repeat Step 2 for the updated B_i until no more non-zero pixels are available for merging into B_i.

Step 4: Setting $i \Leftarrow i+1$ and repeating Steps 1-3 until all non-zero pixels are merged into blocks.

Step 5: The final result consists of a group of non-zero pixel blocks $B_0, B_1, B_2, \mathrm{L}$.

With segmentation processing, the image becomes a collection of pixel blocks that are either target or interference. Target detection for a pixel block is based on pixel concentration level, which may be measured by a metric called *block size*. The block size S_K of a pixel block B_K is defined as the maximum distance of any two pixels inside the block, i.e.

$$S_k = \max_{i,j} \left\| p_i^k , p_j^k \right\|, \ 1 \le i, j \le H \tag{4}$$

where H is the number of pixels in the block B_K.

Based on the block size definition in (4), the following detection criterion is employed to determine whether a block B_K with size S_K in the angle-Doppler domain is a target signal or interference:

$$\begin{aligned} S_K < \beta &\Rightarrow \text{The block is a target} \\ S_K \ge \beta &\Rightarrow \text{The block is interfence} \end{aligned} \tag{5}$$

where the detection threshold β is determined from the image resolution, the number of pulses during a CPI, and the number of antenna array elements. Because an ideal point target signal could occupy up to four resolution cells, the minimum value of β is chosen to be $2r$, where r is the image resolution. With further consideration of such block-expanding factors as windowing, limited numbers of coherent pulses, and antenna array elements, the detection threshold β is selected as:

$$\beta = (4 \sim 8) \cdot r \tag{6}$$

The detection process in (5) is repeated for all pixel blocks in the transformed image.

3. IFSTP Processing Results

We applied the proposed IFSTP algorithm to radar signals generated from a simulated airborne radar system. The radar frequency is 450MHz, the platform height is 9000m and the range is 130km. A linear side-looking antenna array with 32 elements and $\lambda/2$ element spacing is employed. There are 32 coherent pulses in a CPI, and the values of SNR, CNR and JNR per pulse are 0dB, 40dB and 60dB, respectively. The amplitude of the received target signals during a CPI is assumed to be constant.

Figure 2 shows the Fourier transform of radar echoes containing a target, jammer, and clutter. The Doppler frequency of the target is -90Hz and its azimuth is 10°. The jammer is located at an angle of -30°. The radar platform velocity is 50m/s. As a result, the slope of the clutter ridge is one in the angle-Doppler plane.

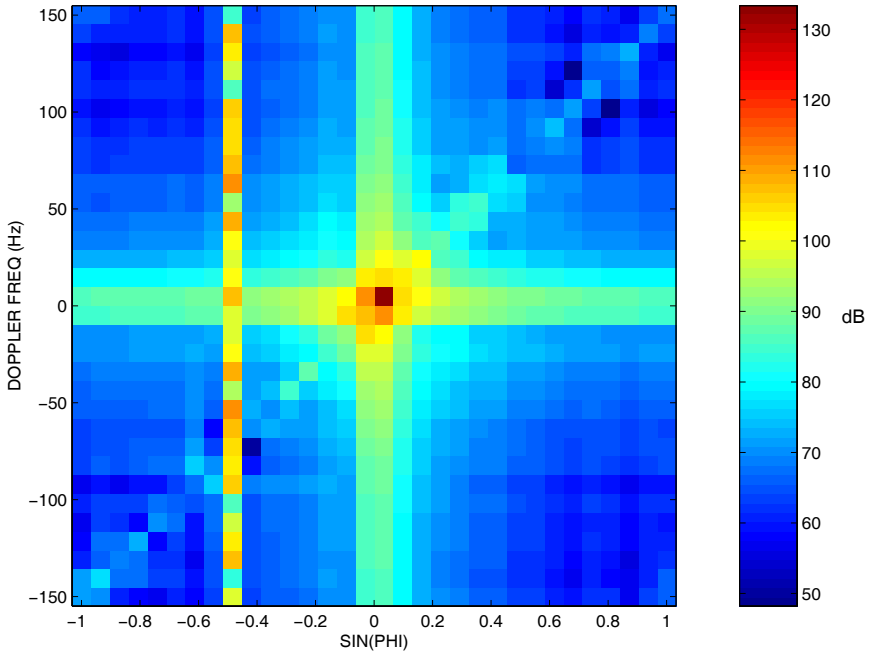

Figure 2: 2-D Fourier transformed image on the Doppler-angle plane for a target with Doppler frequency -90Hz and platform velocity 50m/s.

Because of aliasing effects from the much stronger clutter and jamming, the target signal is not recognizable in Fig. 2. If an 85-dB Chebyshev window is applied to both Doppler and angle domains, and the transformed image is subsequently clamped with the threshold given in (1), the target signal, jammer and clutter ridge become clearly visible, but they are also artificially widened due to the windowing processing. Because of the clutter ridge expansion and $\lambda/2$ array element spacing, some portions of the grating lobes of the clutter ridge appear at the upper-left and lower-right corners of the image. However, they can easily be eliminated as non-targets because they are located at the edges of the image. A more elegant solution is to allow the region growing algorithm to form pixel blocks by warping over the edges of the image, which includes the false target pixels in the interference blocks.

For extraction of target and interference features, the minimum-distance based region growing algorithm, developed in Section II, is applied to the image in Fig. 3.

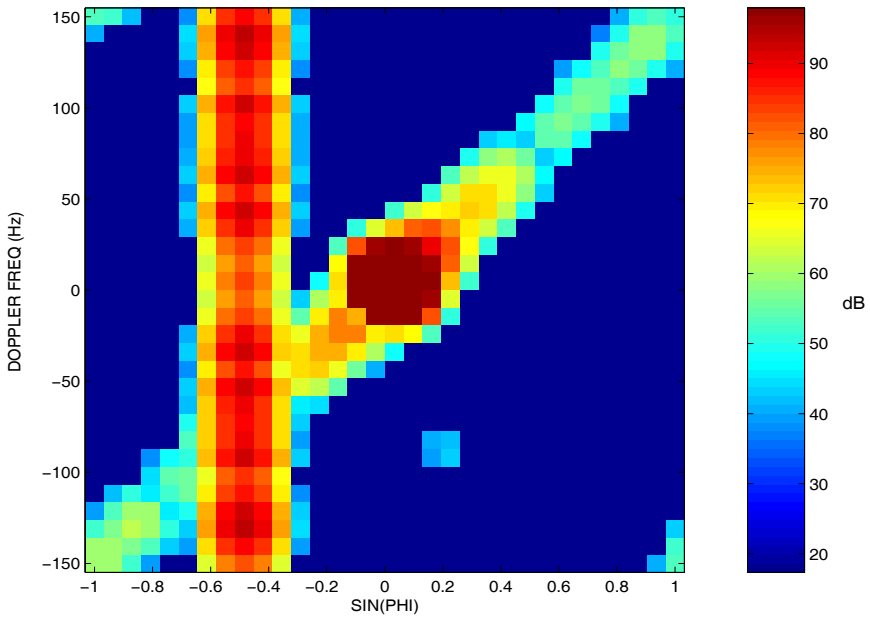

Figure 3: Clamped Doppler-angle image with 85-dB Chebyshev window tapering for radar echo data shown in Fig. 2.

The minimum distance D in (2) is chosen to be two times larger than the image resolution. Such a choice is essential because the amplitude of interference is Rayleigh-distributed and there are some null-points in the sidelobe of the antenna array pattern. The non-zero pixel blocks generated using the region growing are displayed in Fig. 4.

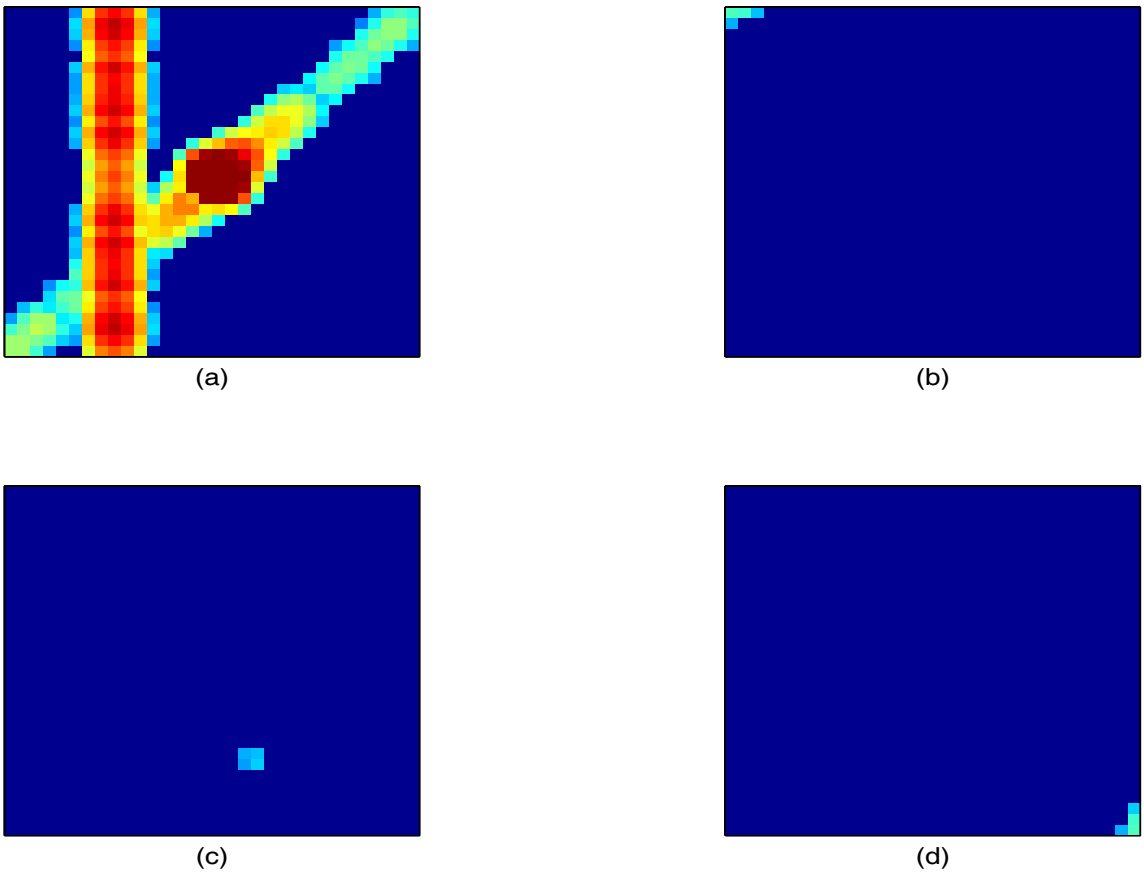

Figure 4: Four pixel blocks generated from the image in Fig. 3 using our minimum-distance based region growing algorithm

Finally, the block-size based target detection scheme in (5) is carried out for all the blocks in Fig. 4. The threshold block size β used for target detection is selected as six. The detection results are listed in Table 1.

Table 1: Block sizes and detection results for the generated pixel blocks in Fig. 4

Block	*a*	*b*	*c*	*d*
Block Size	43.8	2.2	1.4	2.2
Is at Image Edges?	No	Yes	No	Yes
Target?	No	No	Yes	No

Although there are three blocks that meet the target size criterion, two of them are at the image edges and not considered. As shown in Table 1, block *c* is the only target block detected. If the actual target is located at the image edge or overlaps with interference signals, a slightly different radar PRF has to be used to shift the moving target signal away from the interference.

Figure 5 is a generated scene that includes a target and clutter, but no jamming in the angle-Doppler domain. The target Doppler frequency is -125 Hz and its azimuth angle is 0°.

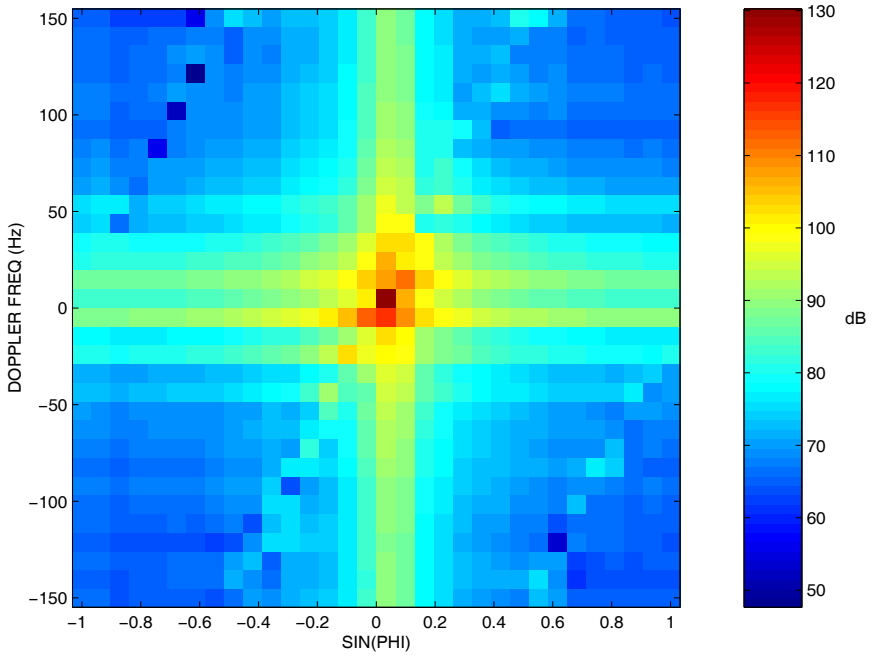

Figure 5: 2-D Fourier transformed image on the Doppler-angle plane for a target with Doppler frequency -125 Hz and platform velocity 100 m/s.

Figure 6 is a post-processing result of the image in Fig. 5, when a Chebyshev window and clamping are applied together.

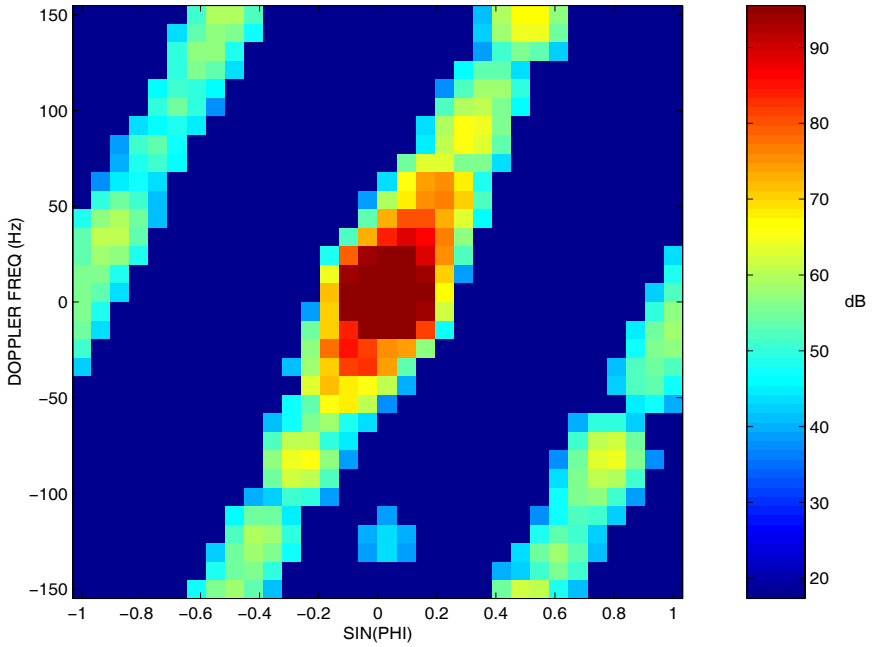

Figure 6: Clamped Doppler-angle image with Chebyshev window tapering for radar echo data shown in Fig. 5.

With the velocity of the radar platform increased to 100m/s, the slope of the clutter ridge in the angle-Doppler plane becomes two, leading to multiple parallel clutter ridges in the transformed image. Likewise, using the region growing algorithm the target and clutter pixel blocks are successfully separated, as shown in Fig. 7.

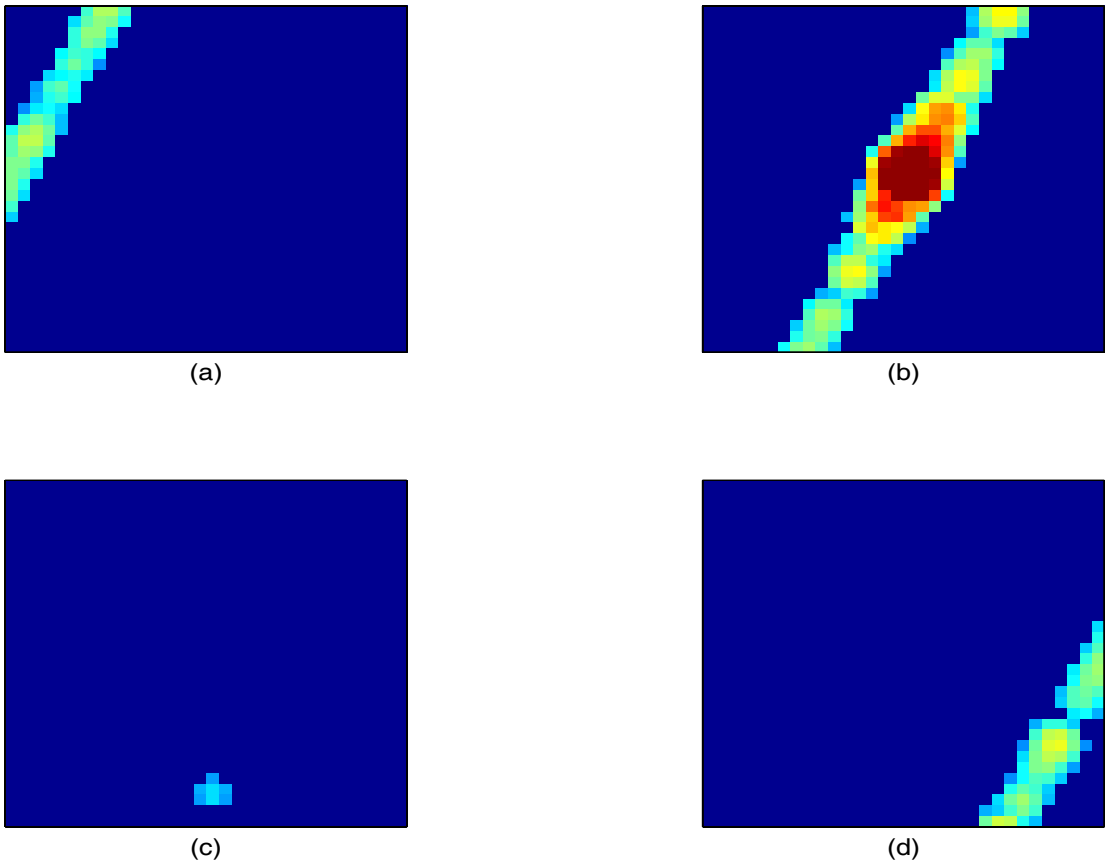

Figure 7: Four pixel blocks generated from the image in Fig. 6, using our minimum-distance based region growing algorithm

With a block-size threshold of 6, the block-size based detection result is listed in Table 2. Block *c* is correctly detected as the target.

Table 2: Block sizes and detection results for the generated pixel blocks in Fig. 7

Block	*a*	*b*	*c*	*d*
Block Size	21.0	36.4	2.2	20.1
Is at Image Edges?	No	No	No	No
Target?	No	No	Yes	No

Conclusions

The Image Feature Based Space-Time Processing (IFSTP) approach is developed as an alternative approach to STAP for moving ground target detection in clutter and jamming. Our simulations suggest that IFSTP can effectively detect moving ground targets based on distinguishing features of targets and interference in the angle-Doppler domain. By avoiding the requirement of estimating clutter statistics, IFSTP is particularly suitable for applications in highly non-homogeneous or unknown clutter environments.

Target detection in IFSTP consists of two steps. The first step is 2-D Fourier transform of data and detecting targets and interference in noise; the second step is extracting targets from interference based on their different features. If targets and interference are clearly separated in the angle-Doppler domain, which is normally true, separating target detection from interference in the second step is very dependable and the overall detection probability and false-alarm rate for IFSTP are basically determined by processing in the first step, i.e., target detection in white noise. Based on the processing described in the first step, the output SNR is maximally increased NM times the input SNR, where N and M are the number of coherent pulses during a CPI and the number of antenna elements, respectively. As a result, the detection performance of IFSTP approaches that of the optimum STAP or matched filter, provided that the targets and interference are clearly separated in the angle-Doppler domain.

Our preliminary analysis also indicates that effects such as sensor crabbing and near-field scattering, which might affect STAP significantly, will not affect IFSTP performance. Although a low PRF is used in our examples, waveforms with high PRF or medium PRF are more desirable for IFSTP because they are more likely to separate

targets further from interferes in the angle-Doppler plane. However, IFSTP is not meant to replace traditional STAP or any other adaptive algorithm. One of obvious shortcomings of IFSTP is that the numbers of array elements and coherent pulses during a CPI need to be large enough to formulate a meaningful image in the angle-Doppler plane. However, this problem could be addressed using super-resolution techniques [9].

References

[1] L. E. Brennan and I. S. Reed, "Theory of adaptive radar," *IEEE Trans. Aerospace and Electronics Systems,* vol.9, pp.237-252, 1973.

[2] H. Wang and L. Cai, "On adaptive spatial-temporal processing for airborne surveillance radar systems," *IEEE Trans. Aerospace and Electronics Systems,* vol. 30, pp.660-669, 1994.

[3] J. Ward, *Space-Time Adaptive Processing for Airborne Radar,* Lincoln Laboratory Technical Report, vol. 10**,** 1994.

[4] A. Haimovich, "The eigencanceler: adaptive radar by eigenanalysis methods," *IEEE Trans. Aerospace and Electronics systems,* vol. 32, pp. 532-542, 1996.

[5] W. Melvin, M. Wicks, P. Antonik, Y. Salama, P. Li and H. Schuman, "Knowledge-based space-time adaptive processing for airborne early warning radar," *IEEE Aerospace and Elec. Sys. Magazine,* vol. 13**,** pp.37-42, 1998.

[6] M. I. Skonlnik, *Introduction to Radar Systems* (Ch. 2), McGraw Hill, New York, 2001.

[7] S. A. Hojjatoleslami and J. Kittler, "Region growing: a new approach," *IEEE Trans. Image Processing,* vol. 7, pp.1079-1084, 1998.

[8] W. K. Pratt, *Digital Image Processing,* Wiley Interscience, New York, 2001.

[9] W. F. Gabriel, "Spectral analysis and adaptive array superresolution techniques," *Proc. of the IEEE,* vol.68, pp. 654-666, June 1980.

PART II: Concurrent Extraction of Target Range and Doppler Information by Using Orthogonal Coding Waveforms

Summary

In this paper, a novel approach for concurrent extraction of target range and Doppler information in radar systems is introduced. A pair of orthogonal waveforms with different pulse repetition frequencies (PRF) are bundled and transmitted as a single hybrid radar waveform for target measurement. At the receiver, two orthogonal signal processing channels consisting of a low PRF and a high PRF channel, perform the extraction of target range and Doppler information, respectively. The CLEAN algorithm is innovatively used to suppress the interference from the cross-correlation residues and the autocorrelation sidelobe in the LPRF channel. The processing results, based on the proposed signal processing approach, demonstrate the technical feasibility of implementing such a signal processing scheme in radar systems.48

1. Introduction

The choice of the radar pulse repetition frequency (PRF) significantly affects the radar performance, relative to the extraction of target information [1-3]. Traditionally, radar systems transmit and process waveforms with fixed PRFs, which may be high, medium or low, during a coherent processing interval (CPI). If a low PRF (LPRF) waveform is used, the target range information is instantly acquired though time delay measurement; while the Doppler frequency, which is readily converted to the radial target velocity due to the target radial motion, is normally ambiguous and not directly measurable. Conversely, if a high PRF (HPRF) waveform is used, the target Doppler shift may be obtained directly through a Fourier transform of the echoes, but the target range becomes ambiguous and has to be indirectly calculated by transmitting multiple staggered PRF waveforms [4, 5]. Thus, for current radar systems, if a waveform with a particular PRF is used for direct measurement of either target range or Doppler shift, the measurement of the other target information is unavoidably indirect, and is thus less accurate and more time-consuming [6, 7]. In other words, existing radar systems do not have the capability to measure target range and velocity simultaneously and accurately. However, for some applications such as tracking high-speed maneuvering targets, it is highly desirable to acquire both target range and velocity simultaneously and instantly [8-10]. In this work, we will demonstrate the technical feasibility of implementing such a radar system by transmitting and processing hybrid radar waveforms consisting of orthogonal coding signals, using both HPRF and LPRF signals.

2. Design and processing of hybrid coding waveform

2.1. Orthogonal coding waveforms

The hybrid coding waveform consists of two different coded sub-waveforms $s_1(t)$ and $s_2(t)$ with one of them transmitted in HPRF and the other in LPRF. The two sub-waveforms should be orthogonal to each other so that they are separable through correlation processing at the receiver for target range/Doppler information extraction, i.e. they should satisfy [11, 12]:

$$\int_t s_1(t) s_2^*(t - t') dt \approx 0 \qquad \forall t' \in R \tag{7}$$

For the transmission and processing of the hybrid waveform to be compatible with current radar system, the two orthogonal coding waveforms are interleaved, bundled and transmitted as a single radar signal, as shown in Figure 8. The sub-waveform $s_1(t)$ in the figure is transmitted with low PRF for instant measurement of target range. The sub-waveform $s_2(t)$ is transmitted with high PRF for direct measurement of target Doppler frequency. The multiple pulses of the coding waveform $s_2(t)$ are fully phase-coherent for pulse Doppler processing at the receiver. The difference between the coding waveform $s_2(t)$ and the coherent pulse train used in regular pulse Doppler radar is that each sub-pulse in $s_2(t)$ is further phase-coded with a code length of *N*.

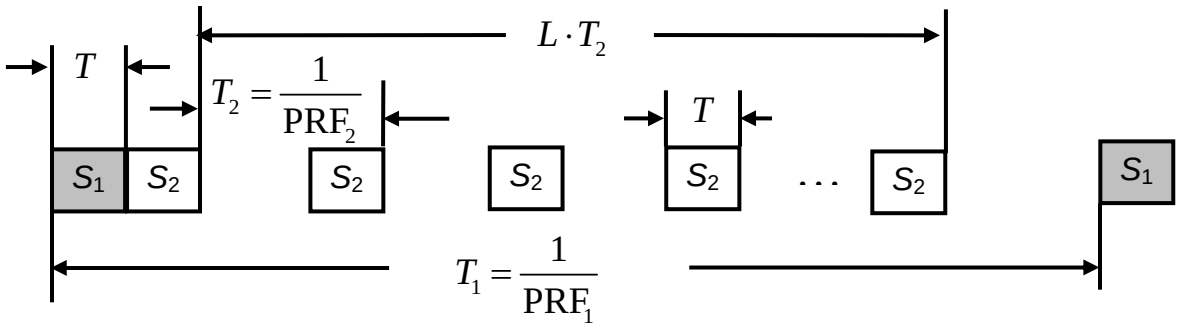

Figure 8: Orthogonal coding waveform containing both HPRF and LPRF sub-waveforms

Assuming that the coding phase sequences for the coding waveforms $s_1(t)$ and $s_2(t)$ are $\{\phi_1(1), \phi_1(2), \mathrm{K}, \phi_1(N)\}$ and $\{\phi_2(1), \phi_2(2), \mathrm{K}, \phi_2(N)\}$, respectively, where N is the code length, the coding waveforms $s_1(t)$ and $s_2(t)$ can be expressed as

$$s_1(t) = \sum_{n=1}^{N} R(t - n\tau) \exp[j\phi_1(n)] \tag{8}$$

and

$$s_2(t) = \sum_{n=1}^{N} R(t - n\tau) \exp[j\phi_2(n)], \tag{9}$$

where τ is the subpulse width of the coding waveforms and $R(t)$ is a rectangular pulse defined as:

$$R(t) = \begin{cases} 1/\tau & 0 \le t < \tau \\ 0 & t \ge \tau \end{cases}. \tag{10}$$

Both waveforms $s_1(t)$ and $s_2(t)$ are assumed to be of pulse duration T, where

$$T = N\tau. \tag{11}$$

The autocorrelation functions of the waveforms $s_1(t)$ and $s_2(t)$ in (2) and (3) and their cross-correlation function are assumed to be $A_1(t)$, $A_2(t)$, and $C(t)$, respectively. Because the two coding signals are orthogonal and possess pseudo-noise characteristic, $A_1(t)$, $A_2(t)$, and $C(t)$ may be approximated as:

$$A_1(t) = \int_{t'} s_1(t') s_1^*(t'+t)\, dt' \approx \begin{cases} N & ;\ t = 0 \\ 0 & ;\ t \neq 0 \end{cases}, \tag{12}$$

$$A_2(t) = \int_{t'} s_2(t') s_2^*(t'+t)\, dt' \approx \begin{cases} N & ;\ t = 0 \\ 0 & ;\ t \neq 0 \end{cases}, \tag{13}$$

$$C(t) = \int_{t'} s_1(t') s_2^*(t'+t)\, dt' \approx 0. \tag{14}$$

The orthogonal waveform containing sub-waveforms $s_1(t)$ and $s_2(t)$, as shown in Fig. 8, is expressed as follows:

$$H(t) = s_1(t) + \sum_{l=1}^{L} s_2(t - T - l.T_2) \tag{15}$$

where L is the number of coherent pulses during a CPI for the waveform $s_2(t)$ and T_2 is the pulse repetition period for the $s_2(t)$ waveform. Because $s_1(t)$ is orthogonal to $s_2(t)$, the target information conveyed in the two signals can be easily separated and extracted at the receiver through a correlation processing.

2.2. Processing of Orthogonal Waveforms for Concurrent Target Range and Doppler Extraction

If a received radar signal contains the echoes from *K* targets during a CPI at an antenna beam dwelling, the amplitudes, initial phases, time delays and Doppler shifts area assumed to be M_k, ϕ_k, τ_d^k, and $f_d^k, k = 1, 2, \mathrm{L}\ , K$, respectively. The received signal prior to the processing is:

$$E(t) = \sum_{k=1}^{K} M_k e^{j\phi_k} s_1\left(t - \tau_d^k\right) e^{j2\pi f_d^k t} + \sum_{k=1}^{K}\sum_{l=1}^{L} M_k e^{j\phi_k} s_1\left(t - T - \tau_d^k - l.T_2\right) e^{j2\pi f_d^k t} . \qquad (16)$$

Because the Doppler shift is normally much smaller than the reciprocal, i.e. 1/*T*, of the duration of the coding signals $s_1(t)$ or $s_2(t)$, its effect on the correlation processing in Fig. 9 is ignored.

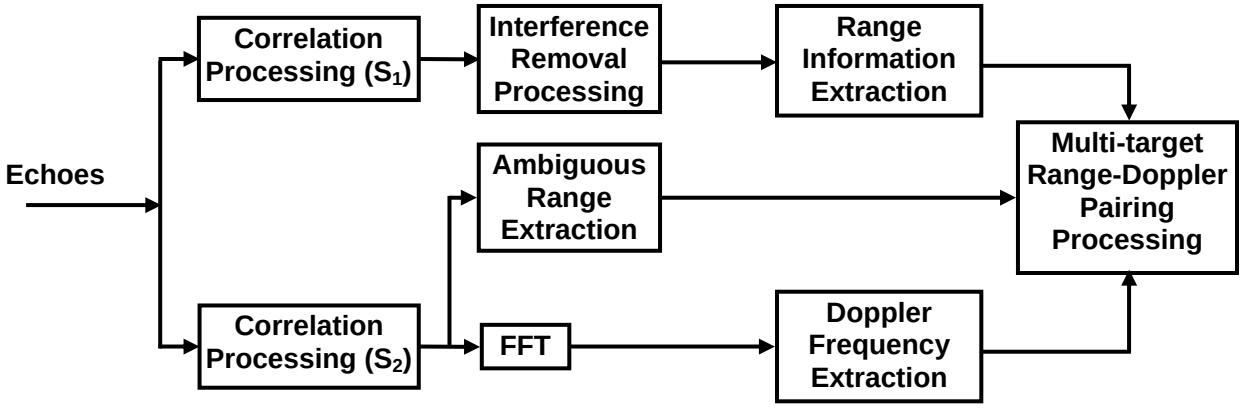

Figure 9: Signal processing scheme for concurrent extraction of target ranges and Doppler frequencies

The target range information, conveyed by the low PRF signal $s_1(t)$ is acquired by correlating the signal in (16) with a correlator matched to $s_1(t)$. This correlator is termed as the low-PRF (LPRF) processor, and its output is given by:

$$P_{LP}(t) \approx \sum_{k=1}^{K} M_k e^{j\phi_k} A_1\left(t-\tau_d^k\right) e^{j2\pi f_d^k t} + \sum_{k=1}^{K}\sum_{l=1}^{L} M_k e^{j\phi_k} C\left(t-T-\tau_d^k - l\cdot T_2\right) e^{j2\pi f_d^k t} \quad . \tag{17}$$

Because $s_1(t)$ and $s_2(t)$ are orthogonal to each other, the magnitude of the output is approximately equal to:

$$\left|P_{LP}(t)\right| \approx \sum_{k=1}^{K} M_k \cdot \left|A_1\left(t-\tau_d^k\right)\right| . \tag{18}$$

The ranges of the radar targets are calculated from the delays of the pulses in (12) from the moment when the waveform is transmitted.

Similarly, a correlator matched to $s_2(t)$ is employed in the high PRF channel to extract target Doppler information from the received signal in (16). The correlation result is:

$$P_{HP}(t) \approx \sum_{k=1}^{K} M_k e^{j\phi_k} C\left(t-\tau_d^k\right) e^{j2\pi f_d^k t} + \sum_{k=1}^{K}\sum_{l=1}^{L} M_k e^{j\phi_k} A_2\left(t-T-\tau_d^k - l\cdot T_2\right) e^{j2\pi f_d^k t} \quad . \tag{19}$$

Because the magnitude of the cross-correlation function C is small and the autocorrelation function A_2 closely approximates the Dirac function, the above equation may be further simplified as:

$$P_{HP}(t) \approx \sum_{k=1}^{K}\sum_{l=1}^{L} M_k e^{j\phi_k} A_2\left(t-T-\tau_d^k - l.T_2\right) e^{j2\pi f_d^k\left(T+\tau_d^k+lT_2\right)} \approx \sum_{k=1}^{K} M_k \cdot e^{j\Phi_k} \sum_{l=1}^{L} A_2(0) e^{j2\pi f_d^k lT_2} , \tag{20}$$

where $\Phi_k = \phi_k + 2\pi f_d^k\left(T+\tau_d^k\right)$ is a fixed value

Generally, the output signal in (20) contains multiple targets locating at different range cells (i.e., time delays). To acquire Doppler information of the k-th target for k = 1, 2, …, K, the signal in (20) is sampled at $t = T + \tau_d^k + l\cdot T_2$; $l = 1, 2, \mathrm{K}, L$, which can be determined using the target range obtained from (12). The Fourier transform is

performed on the *L* sampled data from (20) for each target. If the received signal energy loss due to transmitting eclipse is ignored, the transform result is approximately equal to:

$$\left|FP_{HP}^{k}(f)\right| \approx L \cdot M_k \cdot A_2(0)\delta\left(f - f_d^k\right);\ -1/(2T_2) \le f \le 1/(2T_2);\ k = 1,2,\mathrm{L}\ ,K \qquad (21)$$

where δ is the Dirac function in the frequency domain. Noticeably, the processing result for Doppler information in (17) is much stronger than that for the range information shown in (14) due to the two-time coherent integrations, i.e., correlation and Fourier transform.

For the two-channel processing results of multiple target signals in (18) and (21), the range and Doppler data of the same target are separately obtained, and thus a pairing processing of range and Doppler information is needed for each of the targets. For the high PRF channel processing, the range information in (20) is ambiguous. A simple approach is to use the actual range of a target in (18) to calculate its ambiguous range and perform a Fourier transform only on the data sampled from the ambiguous range unit. An alternative method is to perform the Fourier transform on all ambiguous range units in (20) for the high-PRF channel and to detect all targets with their Doppler frequencies and ambiguous ranges. If a target's Doppler and ambiguous range are f_D and R_A, respectively, its actual range *R* measured using the low PRF channel, is associated with the Doppler frequency f_D by the following equation:

$$R_A = R - \left(\frac{CT_2}{2}\right) \cdot \left\lfloor R \Big/ \left(\frac{CT_2}{2}\right) \right\rfloor \qquad (22)$$

where *C* is the speed of light and $\lfloor x \rfloor$ denotes the largest integer not greater than *x*.

Apparently from (18) and (21), the ranges and the Doppler frequencies of multiple targets are directly and simultaneously measurable by transmitting and processing the orthogonal waveform scheme proposed in this paper. The signal processing scheme for the concurrent range and Doppler measurement is shown in Fig. 9.

2.3. Interference reduction processing using the CLEAN algorithm

The results in (17) and (19) out of the correlation processing in the HPRF and LPRF channels the cross-correlation function $C(t)$ of two orthogonal coding signals $s_1(t)$ and $s_2(t)$ is assumed to be zero and ignored. Because the actual cross-correlation function is not zero, in the multi-target detection case, the cross-correlation residues from strong targets could be comparable to the responses of weak targets, resulting in detection degradation of the weak targets. For the same reason, the sidelobe of a strong target response could interfere with the detection of a weak target. Therefore, the CLEAN algorithm is used to reduce the cross-correlation resides between the HPRF and LPRF waveforms as well as the sidelobes of strong target responses. However, for the HPRF channel processing, the target signal is coherently integrated twice; as a result, even the response of a weak target is normally much stronger than the sidelobe or cross-correlation residues from a strong target. Therefore, interference reduction is only considered for the range information extraction processing (i.e., Low PRF channel).

The CLEAN algorithm has been widely used to remove interference from the autocorrelation sidelobe, using matched processing in the case of weak target detection or clear image formulation [13-17]. In this work, the CLEAN algorithm is adapted to remove both the autocorrelation sidelobe and the cross-correlation residues in the low-

PRF channel. The critical part of implementing the algorithm is to locate the positions of the cross-correlation functions and to determine their magnitudes and phases. The process is to start from the correlation result in the low-PRF channel. For each of the detected targets, there are L (number of the coded pulses for the high-PRF channel) cross-correlation functions that need to be deducted from the result. The location of the cross-correlation functions can be determined from the detected target location in the low-PRF channel and the relative time delays from the low-RPF pulse to the high-PRF pulses. The magnitude can be directly derived from the magnitude of the mainlobe of the target response, while the phase needs to be estimated from the target mainlobe phase and the target Doppler frequency measured in the high-PRF channel. The procedure for implementing the proposed interference reduction method is described below:

STEP 1: If the low-PRF correction processing result is a data sequence $\{d(i)\ i=1,2,3,\mathrm{K}\}$, the strongest target is detected as the index J with magnitude M_J, phase ψ_J, and Doppler frequency f_{JD} (measured at the high-PRF channel), the target sidelobe sequence $\{A'(n); n=1,2,\mathrm{K}\ ,2N-1\}$ is deducted from the data sequence $\{d(i)\}$ with $A'(N)$ aligned to $d(J)$, where the data sequence is derived from the autocorrelation function of the low-PRF coding signal:

$$A'(n)=\begin{cases}\dfrac{M_J e^{j\psi_J}}{N}A_1(n)\ ; & n\neq N\\ 0 & ;\ n=N\end{cases} \tag{23}$$

STEP 2: Subtract the cross-correlation sequence $\left\{C_l^{'}(n)\,;\, n=1,2,\mathrm{K}\,,2N-1\right\}$ between the low-PRF coding pulse and the *l*-th high-PRF coding pulse $(1 \le l \le L)$ from the data sequence $\{d(i)\}$ for the target. The cross-correlation sequence is:

$$C_l^{'}(n) = \frac{M_J e^{j(\psi_J + 2\pi f_{DJ}\cdot\Delta\tau_l)}}{N} C(n) \tag{24}$$

where $\Delta\tau_l$ is the time delay from the low-PRF coding pulse to the *l*-th high-PRF coding pulse of the orthogonal signal, and $C(n)$ is the cross-correction function of $s_1(t)$ and $s_2(t)$.

STEP 3: Repeat the processing in STEP 2 until all cross-correlation resides are removed from the data sequence, i.e. $l=1,2,\mathrm{L}\ ,L$.

STEP 4: Find the next largest target signal from the data sequence and repeat Steps 1-3 until no detectable target signal exists in the data sequence. The final data sequence $\{d(i)\,;\, i=1,2,3,\mathrm{K}\}$ is absent of the autocorrelation sidelobe or the cross-correlation residues.

The uniqueness of the CLEAN algorithm as applied in this work is to subtract the interference from multiple cross-correlation functions rather than the sidelobes of the autocorrelation functions. In addition, to correctly implement the CLEAN algorithm, one needs to estimate and use the target Doppler frequency and the initial phase of the target's echo. Like any other CLEAN algorithm, the processing result is slightly tainted by the inaccuracy of the magnitudes of strong target signals that are affected by additive white noise and the overlapping sidelobe of other nearby targets [17]. Since the

magnitude of the strong target signals is normally much larger than that of white noise or other target sidelobe, the target magnitude distortion is marginal. In this application, the CLEAN result is also inconsequentially affected by the accuracy of the target Doppler frequency estimation in the high-PRF channel.

3. Processing Results

The proposed radar signal processing is applied to the radar data simulated from a scenario with multiple moving targets. The orthogonal waveform is designed using polyphase coding sequences by simulated annealing (SA) [10]. The code length N is 64 and the admissible phase values for the code design are $\left\{ 2\pi l/8 ; l = 0,1,2,\mathrm{K}\ ,7 \right\}$. The relevant parameters of the designed orthogonal waveform shown in Fig.8 are:

- Pulse period of the LPRF waveform $s_1(t)$: T_1 = 8.0ms
- Pulse period of HPRF waveform $s_2(t)$: T_2 = 90μs
- Pulse duration: T = 10μs
- Subpulse duration: $\tau = T/N$ = (5/32)μs
- Number of pulses during a CPI for the HPRF waveform $s_2(t)$: L = 80

It is assumed that the Doppler frequency f_D and the coding signal pulse duration meet the following requirement [18]:

$$f_D \cdot T << 1 \tag{25}$$

3.1. Processing results without interference reduction

If the received radar data contains a single moving target at a range of 150km and Doppler frequency of -2.5kHz, the processing results of the LPRF and HPRF channels are shown in Figs 12 and 11, respectively. The time delay of the target pulse in Fig. 10 from the transmitting time, i.e. at time zero, exactly reflects the target range. Besides the target signal, the interference from the cross-correlation between the LPRF channel signal $s_1(t)$ and the HPRF channel signal $s_2(t)$ is quite visible in the result. This kind of interference signal might mask weak targets and thus preventing them from being detected in the multi-target case.

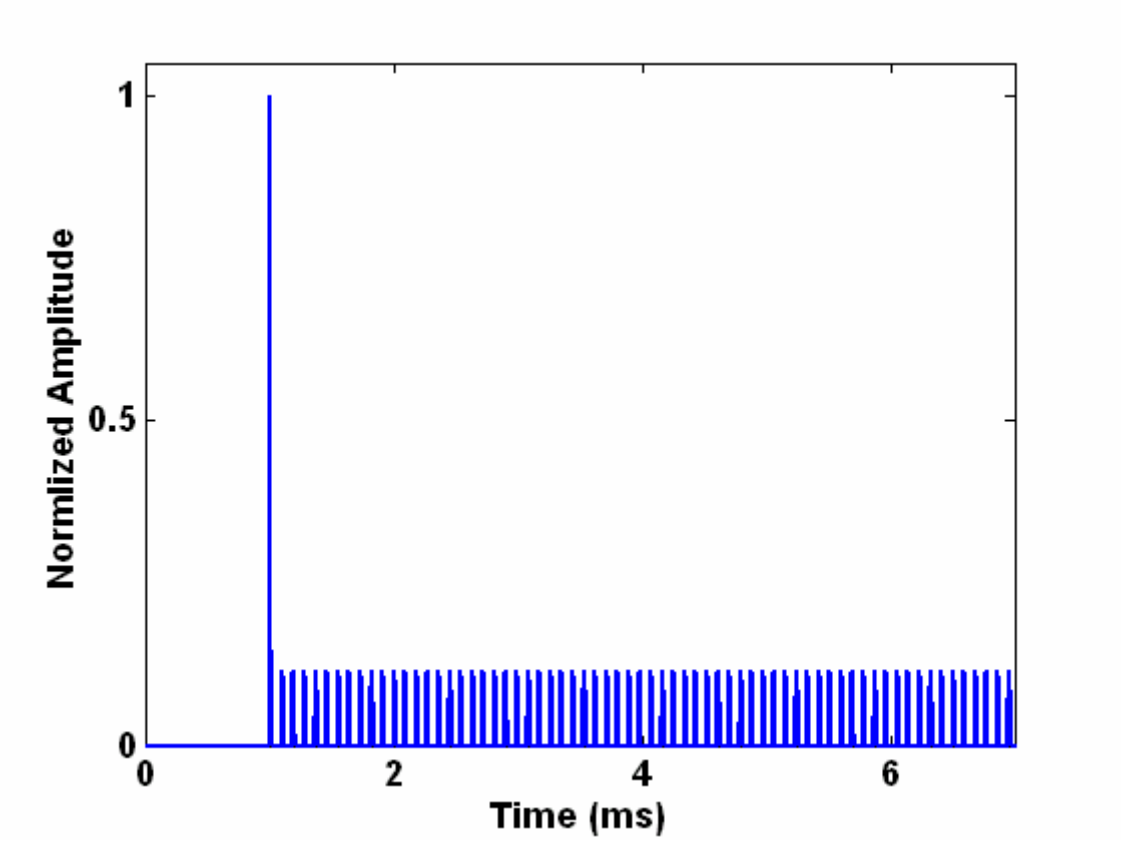

Figure 10: Normalized output of the LPRF processing channel with a single target at a range of 150km

For the HPRF channel processing, Fig. 11 shows the result of Doppler extraction only, based on the data sampled at the target range cell. The Fourier transform results at other range cells are below the target detection threshold. The frequency in Fig. 11 is exactly the target's Doppler frequency -2.5Hz. Due to the two-time coherent integrations for target signal in the HPRF channel, as indicated in (21), the mainlobe of the target signal is much stronger than the sidelobe of the target response and the cross-correlation residues. As a result, the interference is almost indiscernible for the HPRF channel processing result.

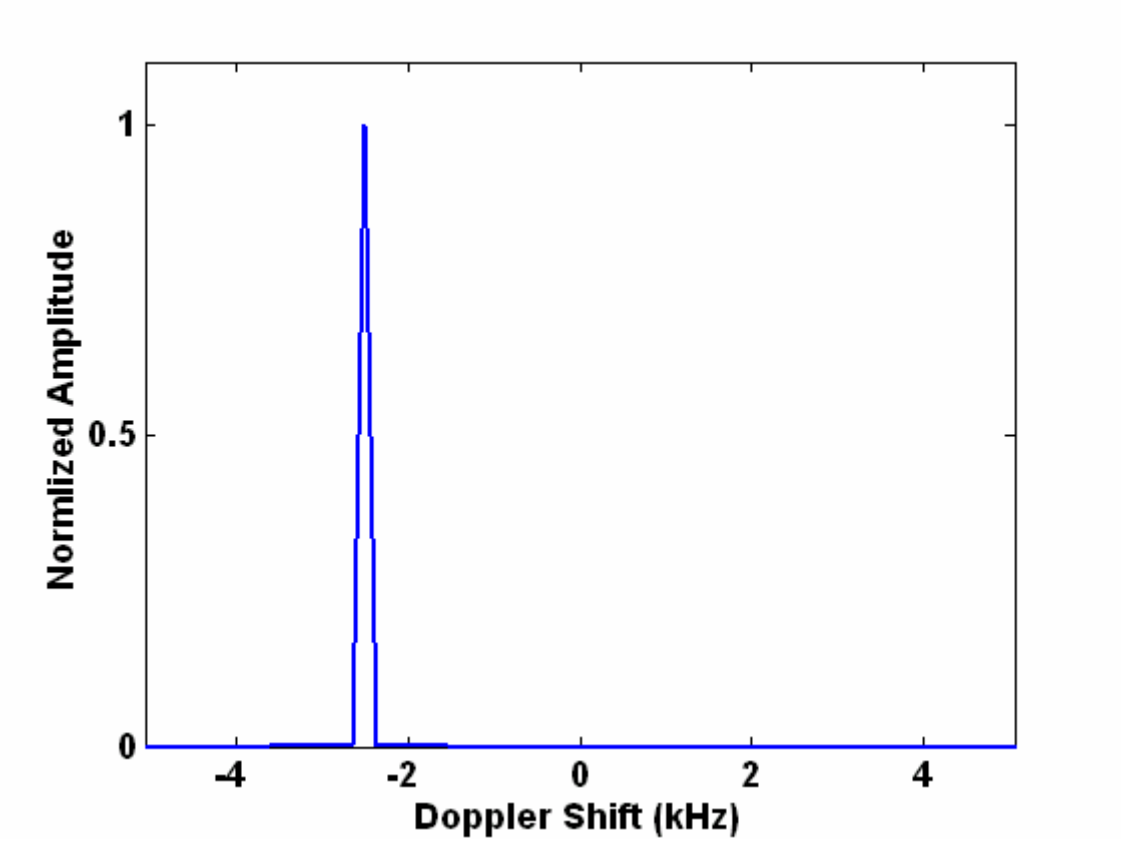

Figure 11: Normalized output of the HPRF processing channel for the same radar data in Fig. 10 containing a single target with Doppler frequency of -2.5kHz.

For practical radar operation, it is most likely that multiple targets exist in the same antenna beam position. Hence, a simulated radar echo containing three moving targets is applied to the proposed signal processing scheme. The ranges of the three targets are 60km, 170km and 350km; their relative magnitudes are 1, 0.8, and 0.5; and their radial Doppler frequencies are 1kHz, 3kHz and -1kHz, respectively. The additive white noise with SNR equal to 14dB is added to the radar data. The low-PRF channel processing result for the multi-target radar signal is shown in Fig. 12. The delayed times for the three targets shown in the figure correspond to their actual ranges. The cross-correlation residues from the HPRF waveform are also observable in the result.

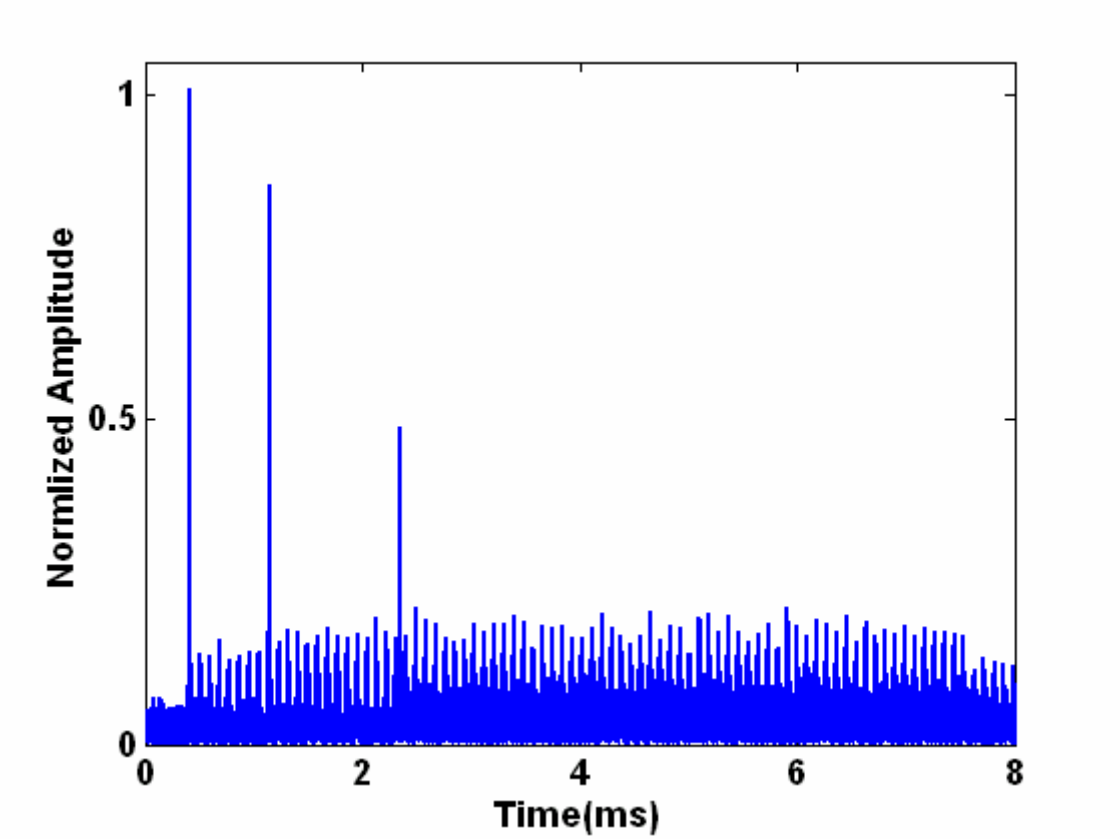

Figure 12: LPRF channel processing result for three targets at ranges 60km, 170km, and 350km and magnitudes of 1, 0.8, and 0.5, respectively. Additive white noise with SNR=14 is included in the input data.

Theoretically, for the HPRF channel processing, the Fourier transform or Fast Fourier Transform (FFT) needs to be performed at all ambiguous range cells during a HPRF CPI, and subsequently target detection is performed at all ambiguous ranges. The processing results, i.e., the target Doppler frequencies, for the ambiguous range cells in which the maximum output value is above the detection threshold are shown in Fig 13.

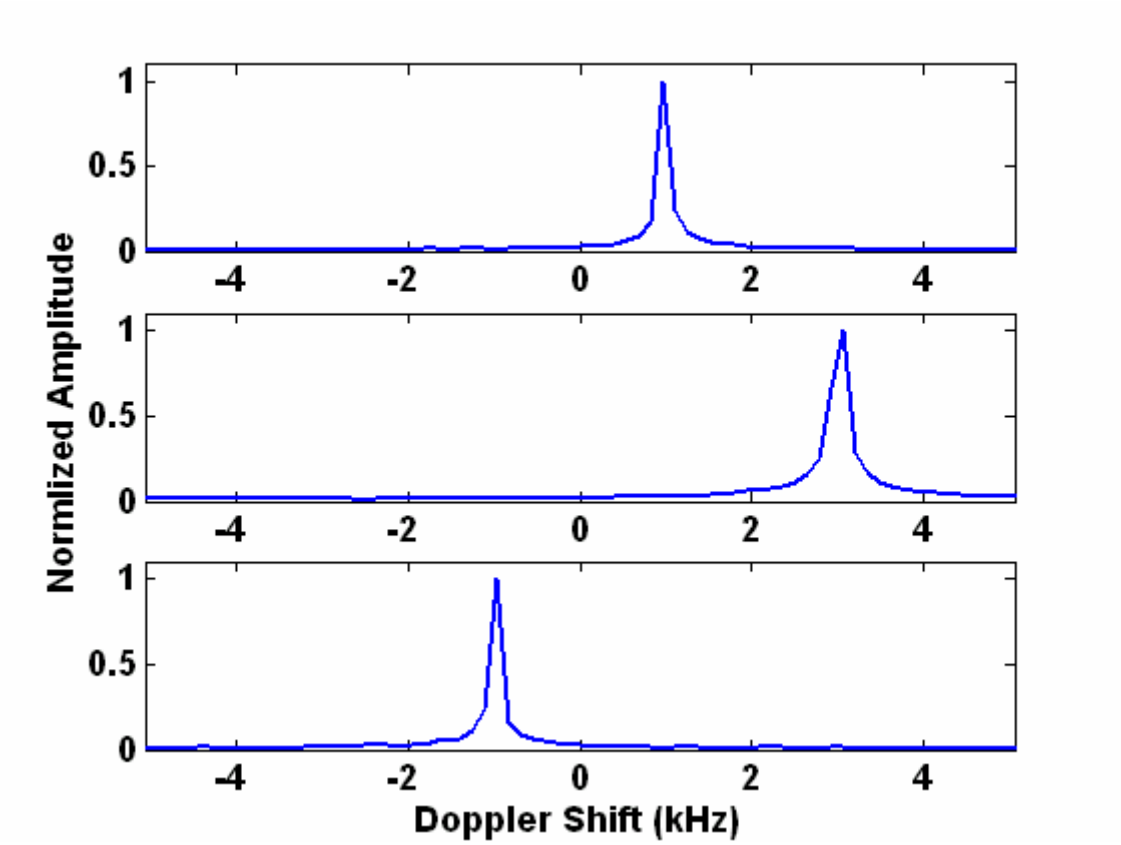

Figure 13: HPRF processing result for the same radar data in Fig. 12 with target Doppler frequencies of 1kHz, 3kHz and -1kHz.

The white noise in the input data has slightly increased the interference level of the processing results in the HPRF and LPRF channels, as shown in Figs 12 and 13, but the overall system performance is not impacted by the additive white noise or any other inference signal in the input data.

The remaining issue in the multiple target detection case is how to associate a range measured in the LPRF channel with a Doppler frequency measured in the HPRF channel for the same target. A straightforward approach is to measure the ranges and the Doppler frequencies separately and independently; and to pair the range and Doppler for each of the targets using (22). The alternative approach is to use the measured range for a target from the LPRF channel to calculate its ambiguous range and perform Doppler processing only at the ambiguous range cells. The latter approach is simple, but slightly delays the execution of Doppler information extraction. Using either approach, one can conveniently find that the range-Doppler pairs from Figs 12 and 13 for the three targets to be: (60km, 1kHz), (170km, 3kHz) and (350km, -1kHz). It is possible that two or more targets may actually have the same ambiguous range, which effectively invalidates either of the two described approaches for pairing the range and the Doppler frequency of a target among multiple targets. In this case, a slightly different PRF has to be used for the HPRF channel to resolve the ambiguous ranges of two or more targets with different ranges.

3.2. Processing result with the CLEAN algorithm applied

In the multiple target scenarios, as discussed in Section II, the detection of the weak target signals in the low-PRF channel could be interfered by the sidelobe of the stronger target responses and the cross-correlation residues between the low-PRF channel correlation filter and the high-PRF coding signals reflected by stronger targets. Fig. 14 shows the LPRF channel processing result for a radar signal containing targets with relative signal magnitudes of 1, 0.8, 0.2 and 0.12. The target ranges are 50km, 120km, 230km and 300km; and their respective Doppler frequencies are 4kHz, -3kHz, 2kHz, and

0.5kHz. With both strong and weak targets existing in the same radar echo, the two weak target signals are completely masked by the sidelobe of the strong target signals and the cross-correlation residues between the LPRF filter and the HPRF waveforms. Therefore, the interference signal needs to be completely removed or at least significantly reduced to effectively detect weak targets. In this work, the CLEAN algorithm is applied to reduce the interference from the LPRF channel processing result. With the interference-suppressed processing, the ranges of the four targets including the weak ones are correctly displayed in Fig. 15. The target Doppler frequencies, which are shown in Fig. 16, are required for correctly implementing the CLEAN algorithm. Note that the CLEAN algorithm does not remove the interference completely because the correlation processing, prior to the CLEAN processing, has slightly distorted the pulse-to-pulse phase shifts caused by the Doppler frequency. In addition, existence of white noise in the received signal also makes perfect interference removal impossible.

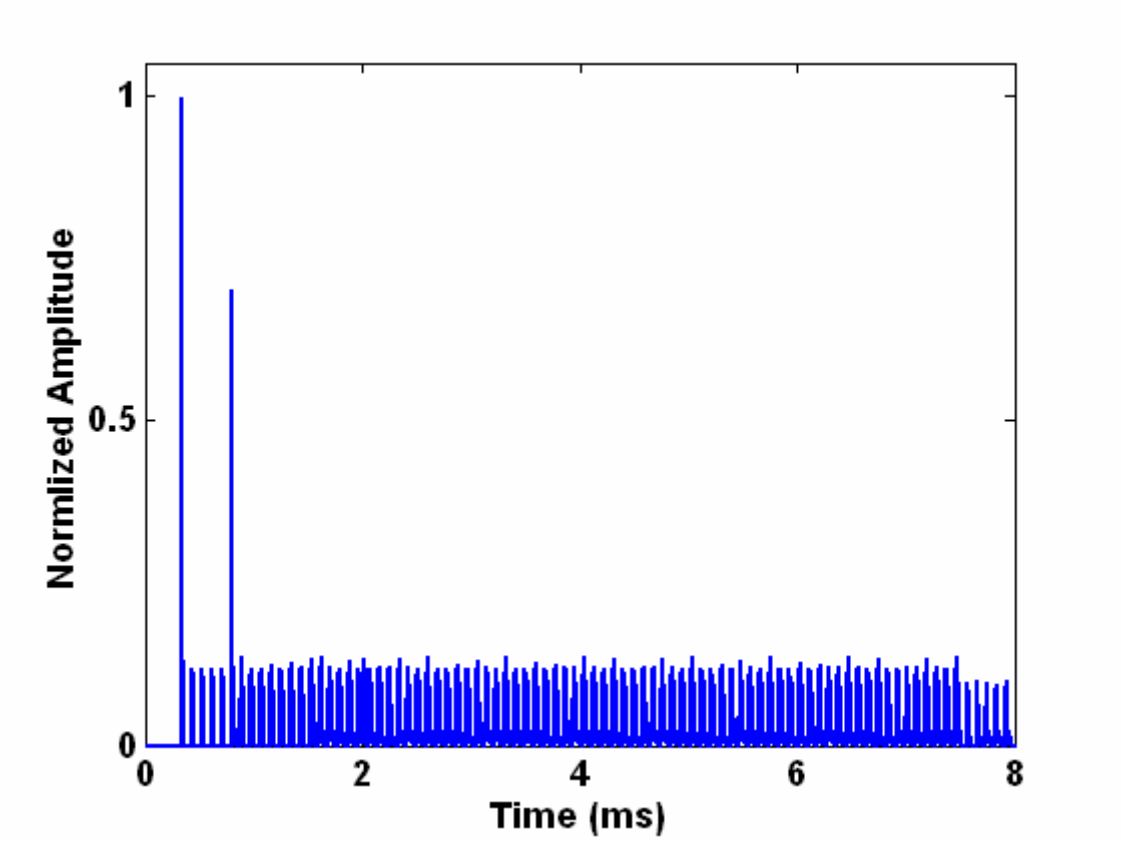

Figure 14: LPRF detection result for four targets with magnitudes of 1, 0.8, 0.2, and 0.12. The two weakest targets cannot be detected due to the interference from cross-correlation residues.

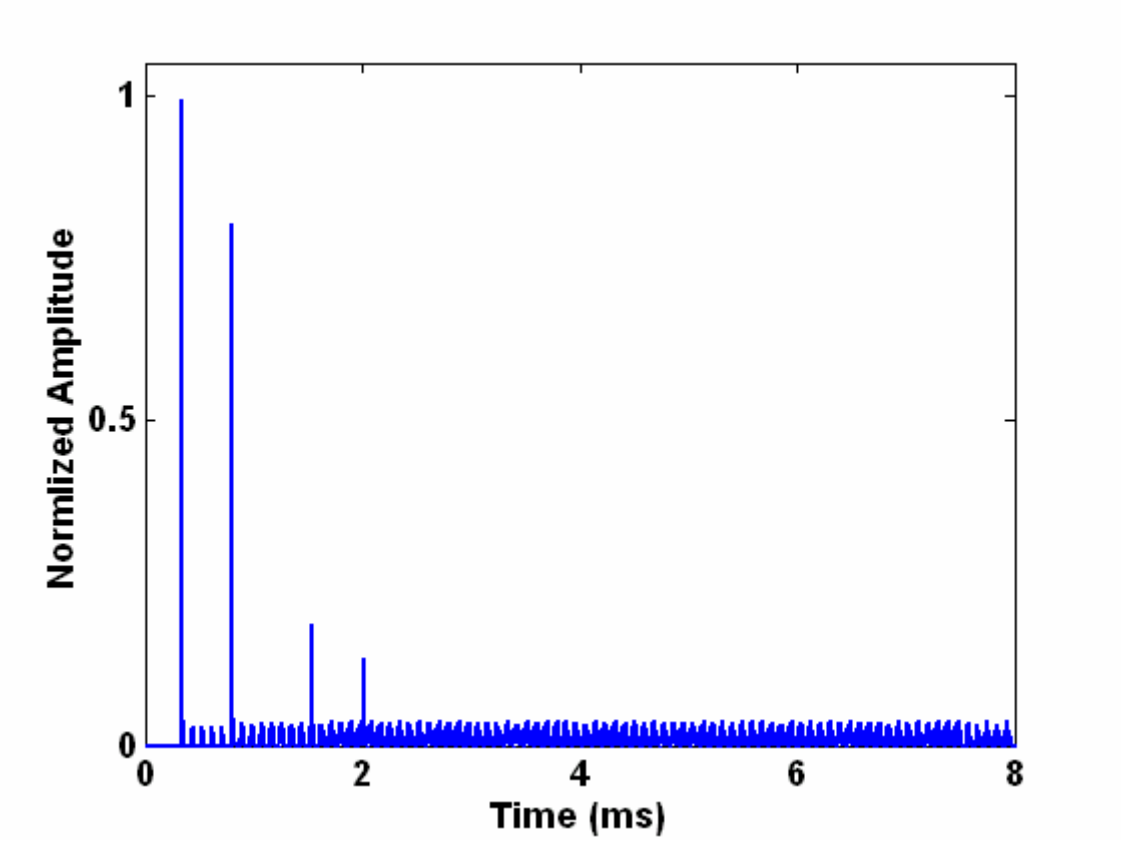

Figure 15: LPRF channel processing result for the same radar data in Fig. 14. The target ranges are 50km, 120km, 230km and 300km. The two weak targets become detectable after interference suppression using the CLEAN algorithm.

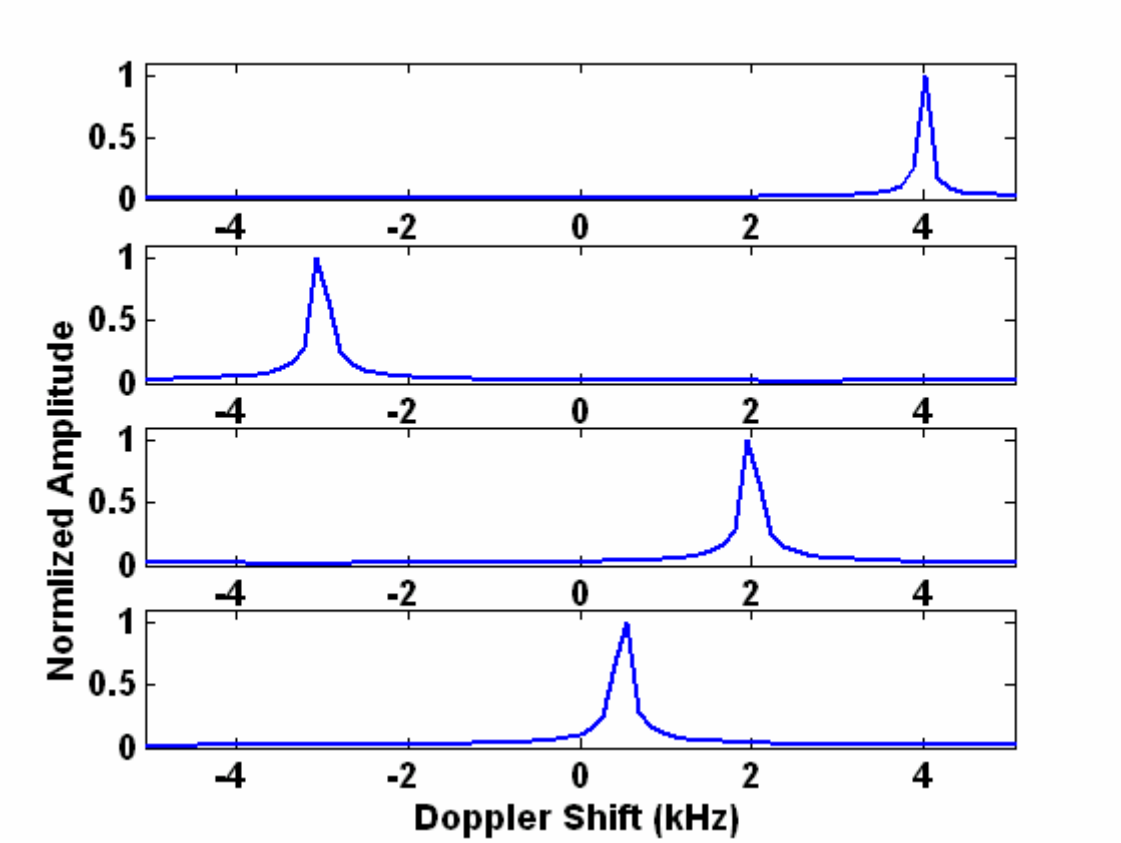

Figure 16: Measured Doppler frequencies of the four targets for the data used in Fig. 14. The extracted Doppler frequencies are 4kHz, -3kHz, 2kHz, and 0.5kHz. The Doppler extraction is performed after interference reduction processing

Figure 17 displays the interference reduction processing for the same input data used in the processing of Fig. 12, which is corrupted by additive white noise. The processing result indicates that the effectiveness of the interference reduction algorithm is not affected by the additive unknown white noise.

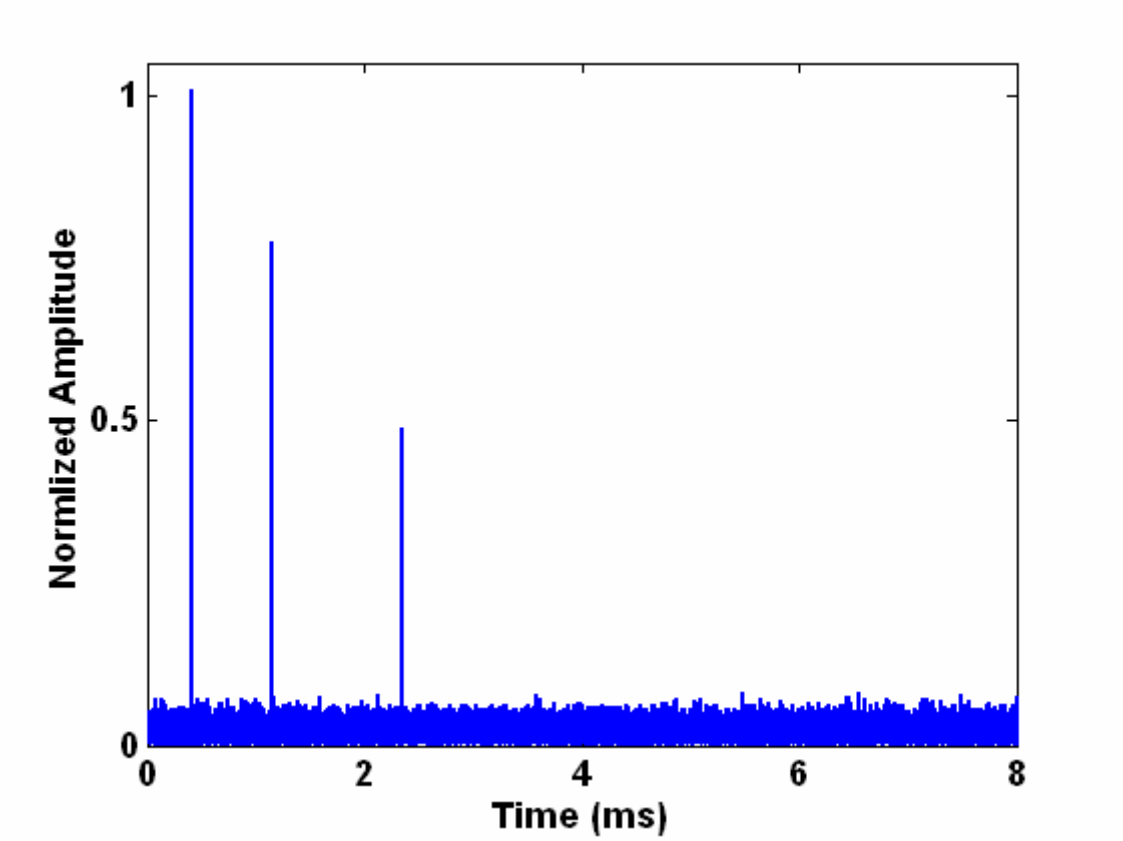

Figure 17: The CLEAN algorithm is applied to the LPRF channel processing result for the same input data as in Fig. 13 with additive white noise in the input data

The computational complexity of implementing the CLEAN algorithm in this work is about $Q \cdot L \cdot 2 \cdot (2N-1)$ additions and multiplications, where Q is the number of targets in a CPI. Because L and N are fixed values and Q is not normally very large for point-target model, the computational cost for using the CLEAN algorithm is not expensive.

4. Conclusions

Theoretical analysis and simulation results have demonstrated that the ranges and velocities of high-speed targets can be concurrently measured by transmitting and processing a specially designed orthogonal waveform scheme. Results show that the proposed signal processing system performs the desired function of concurrent measurement exactly as expected. The application of the CLEAN algorithm is necessary to suppress interference in the LPRF channel for reliable detection of weak targets.

The proposed orthogonal waveform processing scheme is compatible with traditional radar signal processing techniques for clutter rejection such as Moving Target Indication in LPRF channel [2] or Pulse Doppler processing in HPRF channel [7]. They may be directly cascaded to or combined into the proposed signal processing scheme without degrading performance. Therefore, the existence of clutter in the received radar signal does not impair the generality of the proposed algorithm.

The new technique may be applied for effective detection and tracking of high-speed maneuvering targets such as high-speed aircraft and ballistic missiles because of the availability of target range and radial velocity once a target is detected. Similarly, more concurrent radar functions such as target imaging or high-resolution range profiling may be further integrated by including additional orthogonal waveform such as a wideband waveform as part of the transmitting signal and the corresponding processing channel at the receiver. The newly added waveform must be orthogonal to both existing coding waveforms.

For the HPRF channel in the proposed signal processing scheme, due to the two-time integrations, the SNR of the output signal in this channel is much higher than that in

the LPRF channel. If the coding length of the LPRF waveform is designed to be larger, the SNRs of the two channels will be more balanced. Therefore, it is more desirable to design a pair of orthogonal waveforms with different coding lengths in the future.

References

[1]. F. E. Nathanson, *Radar Design Principles,* McGraw-Hill, New York, 1969.

[2]. M. I. Skolnik, *Introduction to Radar Systems* (Ch. 6), McGraw-Hill, New York, 2001.

[3]. D. K. Barton, *Modern Radar System Analysis,* Artech House, Norwood, MA, 1988.

[4]. W. H. Long, D. H. Mooney, and W. A. Skillman, "Pulse Doppler radar," in *Radar Handbook*, 2nd ed., Ch. 17, McGraw-Hill, New York, 1990.

[5]. S. A. Hovanessian, *Introduction to Sensor Systems,* Artech House, Norwood, MA, 1988.

[6]. R. J. Sullivan, *Microwave radar imaging and advanced concepts,* Artech House, Boston, 2000.

[7]. G. E. Stimson, *Introduction to Airborne Radar,* Scitech Publishing, Menhdam, NJ, 1998.

[8]. G. V. Trunk, "Automatic detection, tracking, and sensor integration," in *Radar Handbook*, 2nd ed., pp. 840-848, McGraw-Hill, New York, 1990.

[9]. Hungu Lee and Min-Jea Tahk, "Generalized input-estimation technique for tracking maneuvering targets," *IEEE Trans. Aerospace and Elec. Sys.*, vol. 35, pp. 1388-1402, no. 4, Oct. 1999.

[10]. R. L. Cooperman, "Tactical ballistic missile tracking using the interacting multiple model algorithm," *Proc. of the Fifth International Conference on Information Fusion*, vol.2, pp. 824 – 831, July 2002.

[11]. H. Deng, "Polyphase coding signal design for orthogonal netted radar systems," *IEEE Transactions on Signal Processing*, vol. 52, no. 11, November 2004.

[12]. U. Somaini, "Binary sequences with good autocorrelation and crosscorrelation properties," *IEEE Trans. Aerospace and Elec. Systems,* vol.11, pp 1226-1231, Nov. 1975.

[13]. Högbom, "Aperture synthesis with a non-regular distribution of interferometer baselines," *Astrophys. J. Suppl. Ser.*, vol. 15, pp. 417-426, 1974.

[14]. Y. I. Abramovich, "Compensation methods for the resolution of wideband signals," *Radio Engr. and Elec. Phys.,* vol. 23, pp. 54-59, no. 1, January 1978.

[15]. Y. I. Abramovich and S. A. Zaytesev, “One interpretation of the optimum algorithm for the detection of a signal masked by distributed interfering reflections,” *Radio Engr. and Elec. Phys.*, vol. 23, pp. 25-32, no. 5, May 1979.

[16]. J. Tsao and B. Steinberg, “Reduction of sidelobe and speckle artifacts in microwave imaging: the CLEAN technique,” *IEEE Trans. Antenna and Propagation*, vol. 36, pp. 543-556, April 1988.

[17]. R. Bose, A. Freedman, and B. D. Steinberg, “Sequence CLEAN: a modified deconvolution technique for microwave images of continuous targets,” *IEEE Trans. Aerospace and Elec. Systems*, vol. 38, pp. 89-96, no. 1, Jan. 2002.